Isotropic turbulence surpasses gravity in affecting bubble-particle collision interaction in flotation

Duc Ngo-Cong[a,*], Anh V. Nguyen [b,*] and Thanh Tran-Cong [a,c]

[a] Computational Engineering and Science Research Centre, University of Southern Queensland, Toowoomba, QLD 4350, Australia.

[b] School of Chemical Engineering, The University of Queensland, Brisbane, QLD 4072, Australia.

[c] School of Mechanical and Electrical Engineering, Faculty of Health, Engineering and Science, University of Southern Queensland, Toowoomba, QLD 4350, Australia.

ABSTRACT

Turbulence and mechanical flotation cells have been the workhorse of the mining industry to process the high tonnage but low-grade ores for more than a century. However, our quantitative understanding of the effect of turbulence on flotation is still limited. Here we theoretically investigate the bubble-particle collision in flotation in homogeneous isotropic turbulence using the correlation method. We show a novel paradigm that isotropic turbulence can surpass gravity in affecting bubble-particle collision in flotation. Specifically, motions of particles of micrometer sizes and bubbles of millimeter sizes are described using the Basset-Boussinesq-Oseen equation. The drag forces on particles and bubbles are calculated using Stokes' law with a particle-size correction factor and Allen's law, respectively. The correlation method is applied to determine bubble and particle velocity variances and covariances. The collision kernel is then calculated, taking into account the effects of turbulence acceleration and shear, and gravity of the bubble-particle system. We compare our collision model with the available models and investigate the influence of bubble and particle sizes, particle density and dissipation rate of turbulent kinetic energy on the collision kernel. The results show that the bubble-particle collision kernel increases with increasing bubble and particle sizes, and dissipation rate of turbulent kinetic energy. Importantly, turbulence can significantly enhance the collision efficiency, exceeding the ideal rate of collision by gravity and leading to the turbulence collision efficiency greater than unity.

Keywords: bubble-particle interaction; correlation method; turbulent motion; BBO equation

*Correspondence: duc.ngo@usq.edu.au (Duc Ngo-Cong), anh.nguyen@eng.uq.edu.au (Anh V. Nguyen)

1. INTRODUCTION

Different types of flotation cells have been invented since the invention of froth flotation (Lynch et al., 2010; Nguyen and Schulze, 2004). Of these cells, the mechanical cells have dominated the industry since the beginning. It is very unlikely that these mechanical cells are going to be replaced by different cell types because of the demand to process the high tonnage of low-grade ores which has led to the current use of very large cells (> 500 m^3). Special cell designs such as flotation columns, Microcels and Jameson cells fulfill the special need of the industry for coal flotation or special cleaning circuits.

In a mechanical flotation cell, air is introduced into the cell near the impeller to form fine bubbles of millimeter size under the mixing effect of the impeller. The rising fine bubbles collect and carry hydrophobic particles (valuable particles) to form a froth layer and exit to the launders while hydrophilic particles (gangue particles) sink to the bottom of the cell to be rejected (Napier-Munn and Wills, 2006). A turbulent flow is claimed to be beneficial to bubble-particle collision and attachment. However, the turbulent effect can cause coarse particles with a high inertia to detach from bubbles, which decreases the flotation efficiency. Three major bubble-particle interaction sub-processes, namely, collision, attachment, and detachment, can be treated separately since their governing forces are independent of each other (Nguyen and Schulze, 2004).

In the literature, the model development of bubble-particle collision in turbulent flow is very limited when compared to that of droplet-droplet collision (Hu and Mei, 1997; Panchev and Haar, 1971; Pinsky et al., 2006; Saffman and Turner, 1956; Wang et al., 1998) or/and particle-particle collision (Abrahamson, 1975; Alipchenkov and Zaichik, 2003; Ayala et al., 2008; Kruis and Kusters, 1997; Meyer and Deglon, 2011; William and Crane, 1983; Yuu, 1984) in gas-particle flows. We note that these available models developed by considering the similar sizes of droplets or solid particles are physically inconsistent with bubble-particle interactions in flotation which have different sizes with different orders of magnitudes (Meyer and Deglon, 2011). Saffman and Turner (1956) derived a collision model of droplets in the turbulent cloud for the limit of small particles which are perfectly correlated with the surrounding carrier fluid. Abrahamson (1975) suggested a model for the limit of very high inertial particles whose velocities are completely

uncorrelated with the surrounding carrier fluid. Since the particle density is assumed to be much larger than that of the carrier fluid, these models are not applicable to the particle-liquid system where the liquid density has the same order as the particle density. Yuu (1984) developed an expression for the fluctuating relative velocity of two inertial particles taking into account the relative velocity between fluid and particle, and the added mass effect experienced by solid particles in a liquid system. He found that the collision due to the spatial variation of turbulence was the predominant factor for small inertial particles in a water stream. However, the particle motion relative to water still increases the collision rate by about 20%.

There have been many deterministic models for bubble-particle collision efficiency available in the literature (Dai et al., 2000; Nguyen et al., 2016). In order to investigate the influence of microturbulence on bubble-particle collision in flotation, a stochastic approach to modeling turbulent flows is highly necessary (Nguyen et al., 2016). Schubert et al. (Schubert, 1996; Schubert, 1999; Schubert and Bischofberger, 1978, 1998; Yoon, 2000) were the first to consider and quantify the effect of turbulence in flotation. Typically, turbulence was considered to affect the collision rate between bubbles and particles in flotation. Modifying the collision rate derived for the particle-particle interaction by Abrahamson (Abrahamson, 1975), Schubert (Schubert, 1999) obtained the following expression for the bubble-particle collision frequency (i.e., the number of collision per unit volume and time):

$$\Gamma = 5 n_p n_b \left(R_p + R_b \right)^2 \sqrt{\overline{\mathrm{v}'^2_p} + \overline{\mathrm{v}'^2_b}} \tag{1}$$

where n_p and n_b are the particle and bubble number concentrations, respectively, R_p and R_b are the particle and bubble radii, $\overline{\mathrm{v}'^2_p}$ and $\overline{\mathrm{v}'^2_b}$ are the root-mean-square values of the turbulent velocity fluctuations of the particles and bubbles, respectively, relative to the turbulent fluid velocity. Using Kolmogorov's theory of isotropic turbulence, these velocities can be connected with the rate dissipation energy, ε, within the flotation cell, giving the following equation (Schubert, 1999):

$$\overline{\mathrm{v}'^2_i} = 0.33 \frac{\varepsilon^{4/9} \left(2R_i \right)^{7/9}}{\left(\rho / \mu \right)^{1/3}} \left(\frac{\rho_i - \rho}{\rho} \right)^{2/3} \tag{2}$$

where ρ is the liquid density, μ is the liquid dynamic viscosity and the index "*i*" can be "*p*" or "*b*" for particles and bubbles, respectively. Many other expressions for the turbulent collision rates between particles or droplets are recently reviewed (Meyer and Deglon, 2011). Schubert et al.'s approach to quantifying the effect of turbulence in flotation was re-applied and re-analyzed by a number of researchers (Jameson et al., 2007; Pyke et al., 2003; Yoon, 2000). In these studies, the effect of turbulence on flotation was incorporated into the bubble-particle collision frequency which is an important term of the rate constant of flotation kinetics in a mechanical cell. Specifically, turbulence has not been considered in predicting the bubble-particle collision efficiency. The available models for the collision efficiency are based on the deterministic collision interaction unaffected by the stochastic interactions with turbulence.

In the present study, we focus on modeling the bubble-particle collision rate and efficiency by taking into account the dependence of colliding particle and bubble velocities through the covariance of bubble-particle fluctuating velocities. We apply the correlation method to derive new expressions for the bubble-particle velocity covariance and related models.

2. MODELLING OF BUBBLE-PARTICLE COLLISION IN ISOTROPIC TURBULENCE

When dealing with turbulent motions, it is customarily to apply the Reynolds decomposition, whereby instantaneous quantities are decomposed into their time-averaged and fluctuating quantities. For turbulent bubble-particle collision interaction, it is shown previously (Nguyen et al., 2016) that the Reynolds decomposition can be used to decompose the bubble-particle relative velocity into the time-averaged (deterministic) and fluctuating (stochastic) components. This decomposition splits the collision efficiency into two terms: the collision efficiency due to the time-averaged (mean) interactions and the collision efficiency due to the fluctuating relative motion between the bubble and particles. The results for the time-averaged interactions are reviewed previously. Here our focus is on the collision efficiency due to the fluctuating relative motion between the bubble and particles. Therefore, if not otherwise stated, all velocity components (and many other variables) in this paper are the fluctuating quantities.

The bubble-particle collision rate is defined as the number of particles colliding with a bubble per unit time (Nguyen and Schulze, 2004),

$$N_c = \oint \mathbf{J} \cdot d\mathbf{S}_b = n_p \oint \mathbf{W} \cdot d\mathbf{S}_b = n_p \Gamma \qquad (3)$$

where n_p is the particle number density; $\mathbf{J}$ the particle flux vector; $d\mathbf{S}_b$ the bubble surface element vector; $\mathbf{W}$ the bubble-particle relative velocity vector; and Γ the bubble-particle collision kernel defined by

$$\Gamma = \oint \mathbf{W} \cdot d\mathbf{S}_b \tag{4}$$

Following the available literature (Nguyen and Schulze, 2004), the ideal rate of bubble-particle collision in flotation is determined by the ideal relative motions of bubbles and particles by gravity and described by

$$N_{ci} = n_p \Gamma_i = n_p \pi R^2 \left(V_{pz} + V_{bz} \right) \tag{5}$$

where V_{pz} and V_{bz} are the terminal velocities of particle settling and bubble rising, respectively, and $R = R_p + R_b$. The collision efficiency is determined as

$$E_c = \frac{N_c}{N_{ci}} = \frac{\Gamma}{\pi R^2 \left(V_{pz} + V_{bz} \right)} \tag{6}$$

For simplicity, we use the following expressions for calculating the particle and bubble terminal velocities (Nguyen and Schulze, 2004):

$$V_{pz} = \frac{2R_p^2 (\rho_p - \rho) g}{9\mu} \left\{ 1 + \frac{Ar}{96} \left[1 + 0.079 \left(Ar \right)^{0.749} \right]^{-0.755} \right\}^{-1} \tag{7}$$

$$V_{bz} = \frac{4R_b^2 \rho g}{\mu} \left\{ \frac{4a^2 \left(Ar_* \right)^{2b-1} Mo^{0.46b}}{3k} \right\}^{\frac{1}{2-2b}} \tag{8}$$

where $Ar = 8R_p^3 \left(\rho_p - \rho \right) \rho g / \mu^2$ and $Ar_* = 8R_b^3 \rho^2 g / \mu^2$ are the Archimedes numbers for the particles and bubbles, respectively, and $Mo = g\mu^4 / (\rho\sigma^3)$ is the Morton number. The numerical constants (*a*, *b* and *k*) on the right-hand side of Eq. (8) are given, as a function of the bubble Archimedes number, in Table 5.1 of Nguyen and Schulze (Nguyen and Schulze, 2004). It is also noted that Eq. (8) is valid for the air bubbles with their Reynolds numbers being larger than 130. For the bubbles with smaller Reynolds numbers, one can apply Eq. (7) where the density

difference, $\rho_p - \rho$, in Eq. (7) and *Ar* by the liquid density, ρ.

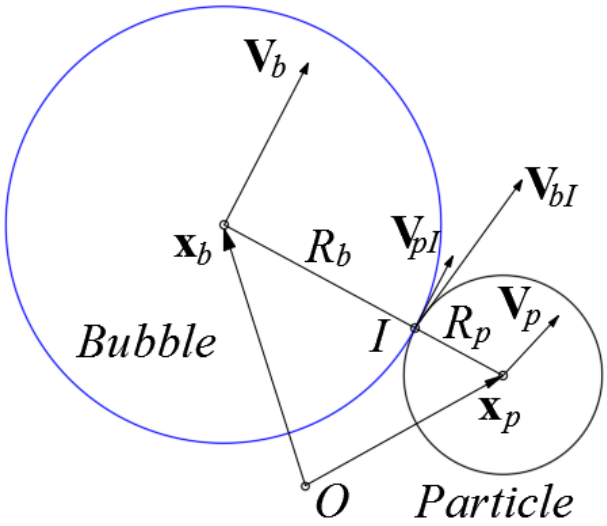

Figure 1. A bubble-particle collision model (not to scale), designed relative to an origin *O*.

The velocity vectors of a bubble and a particle with their centers at the position $\mathbf{x}_b$ and $\mathbf{x}_p$ (Fig. 1) are determined using a Taylor expansion as follows (Yuu, 1984):

$$\mathbf{V}_b = \mathbf{V}_{bI} \mp \mathbf{R}_b \cdot \frac{\partial \mathbf{V}_{bI}}{\partial \mathbf{s}} \tag{9}$$

$$\mathbf{V}_p = \mathbf{V}_{pI} \pm \mathbf{R}_p \cdot \frac{\partial \mathbf{V}_{pI}}{\partial \mathbf{s}} \tag{10}$$

where $\mathbf{V}_b$ and $\mathbf{V}_p$ are the velocity vectors of the bubble and the particle at their positions $\mathbf{x}_b$ and $\mathbf{x}_p$, respectively; $\mathbf{V}_{bI}$ and $\mathbf{V}_{pI}$ are the velocity vectors of the bubble and the particle at the contact point I; $\mathbf{R}_b = \left(R_{bx}, R_{by}, R_{bz}\right)$ and $\mathbf{R}_p = \left(R_{px}, R_{py}, R_{pz}\right)$. Here we only deal with spherical particles and bubbles. For non-spherical particles and bubbles, the size of particles and bubbles could be replaced by their volume-equivalent diameter.

The variance of bubble-particle relative velocity $\overline{\mathbf{W}^2}$ is calculated as follows:

$$\overline{\mathbf{W}^2} = \overline{\left(\mathbf{V}_p - \mathbf{V}_b\right)^2} = \overline{\mathbf{V}_p^2} + \overline{\mathbf{V}_b^2} - 2\overline{\mathbf{V}_p}\,\overline{\mathbf{V}_b}\,. \tag{11}$$

Substitution of Eqs. (9) and (10) into Eq.(11) gives

$$\begin{aligned}\overline{\mathbf{W}^2} = \overline{\left(\mathbf{V}_{pI} - \mathbf{V}_{bI}\right)^2} + \overline{\left(\mathbf{R}_p \cdot \frac{\partial \mathbf{V}_{pI}}{\partial \mathbf{s}}\right)^2} + \overline{\left(\mathbf{R}_b \cdot \frac{\partial \mathbf{V}_{bI}}{\partial \mathbf{s}}\right)^2} + 2\overline{\left(\mathbf{R}_p \cdot \frac{\partial \mathbf{V}_{pI}}{\partial \mathbf{s}}\right)\left(\mathbf{R}_b \cdot \frac{\partial \mathbf{V}_{bI}}{\partial \mathbf{s}}\right)} \\ \pm 2\overline{\left(\mathbf{V}_{pI} - \mathbf{V}_{bI}\right)\left(\mathbf{R}_b \cdot \frac{\partial \mathbf{V}_{bI}}{\partial \mathbf{s}} + \mathbf{R}_p \cdot \frac{\partial \mathbf{V}_{pI}}{\partial \mathbf{s}}\right)}\end{aligned} \tag{12}$$

The real variance of $\overline{\mathbf{W}^2}$ is the arithmetic average of two cases expressed by the plus/minus sign in Eq. (12). Thus, we obtain

$$\overline{\mathbf{W}^2} = \overline{\mathbf{V}_{bI}^2} + \overline{\mathbf{V}_{pI}^2} - \overline{2\mathbf{V}_{pI}\mathbf{V}_{bI}} + \overline{\left(\mathbf{R}_b \cdot \frac{\partial \mathbf{V}_{bI}}{\partial \mathbf{s}}\right)^2} + \overline{\left(\mathbf{R}_p \cdot \frac{\partial \mathbf{V}_{pI}}{\partial \mathbf{s}}\right)^2} + \overline{2\mathbf{R}_p \cdot \frac{\partial \mathbf{V}_{pI}}{\partial \mathbf{s}}\mathbf{R}_b \cdot \frac{\partial \mathbf{V}_{bI}}{\partial \mathbf{s}}}\,. \tag{13}$$

2.1. Particle motion equation

The particle motion equation is written in the absence of the Basset history force and the gravitational force as follows (Abrahamson, 1975; Nguyen et al., 2016):

$$\frac{\pi d_p^3}{6}\rho_p \frac{d\mathbf{V}_p}{dt} = \underbrace{\mathbf{F}_{Dp}}_{drag\ force} + \underbrace{\frac{\pi d_p^3}{6}\rho \frac{d\mathbf{V}}{dt}}_{pressure\ force} + \underbrace{\frac{\pi d_p^3}{12}\rho\left(\frac{d\mathbf{V}}{dt} - \frac{d\mathbf{V}_p}{dt}\right)}_{added\ force}. \tag{14}$$

The viscous drag acting on a particle is determined by

$$\mathbf{F}_{Dp} = 6\pi\mu R_p f_p\left(\mathbf{V} - \mathbf{V}_p\right) \tag{15}$$

where $f_p = 1 + 0.169\,\mathrm{Re}_p^{2/3}$ (for $0 < \mathrm{Re}_p \le 700$) is the correction factor to Stokes' law for drag, and $\mathrm{Re}_p = 2R_p\left|\mathbf{V}_p - \mathbf{V}\right|/\nu$ is the particle Reynolds number.

The particle motion equation (14) can be rewritten as follows:

$$\frac{d\mathbf{V}_p}{dt} + a_p\mathbf{V}_p = a_p\mathbf{V} + b_p\frac{\partial \mathbf{V}}{\partial t}, \tag{16}$$

where reciprocal relaxation time a_p and the buoyancy coefficient b_p are given by

$$a_p = \frac{36\mu f_p}{d_p^2\left(2\rho_p + \rho\right)} \tag{17}$$

$$b_p = \frac{3\rho}{\left(2\rho_p + \rho\right)}. \tag{18}$$

For simplicity, Eq. (16) is rewritten as follows:

$$\frac{dV_{pi}}{dt} + a_p V_{pi} = a_p V_i + b_p \frac{\partial V_i}{\partial t}, \tag{19}$$

where V_{pi} and V_i are the particle and liquid fluctuating velocities in the i^{th} direction, respectively.

2.2. Bubble motion equation

The bubble motion equation is described in the absence of the Basset history force and the gravitational force as follows:

$$\frac{\pi d_b^3}{6}\rho_b \frac{d\mathbf{V}_b}{dt} = \underset{drag\ force}{\mathbf{F}_{Db}} + \underbrace{\frac{\pi d_b^3}{6}\rho \frac{d\mathbf{V}}{dt}}_{pressure\ force} + \underbrace{\frac{\pi d_b^3}{12}\rho\left(\frac{d\mathbf{V}}{dt} - \frac{d\mathbf{V}_b}{dt}\right)}_{added\ force}. \tag{20}$$

The drag acting on the bubble is determined by

$$\mathbf{F}_{Db} = 6\pi\mu R_b f_b\left(\mathbf{V} - \mathbf{V}_b\right). \tag{21}$$

where $f_b = 5\mathrm{Re}_b^{1/2}/12$ is the factor of the drag correction and Re_b is the bubble Reynolds number. Similarly to Eq. (19), the composite expression of Eq. (20) gives

$$\frac{dV_{bi}}{dt} + a_b V_{bi} = a_b V_i + b_b \frac{\partial V_i}{\partial t} \tag{22}$$

where V_{bi} is the bubble fluctuating velocity in the *i*-direction and the parameters are given as follows:

$$a_b = \frac{36\mu f_b}{d_b^2\left(2\rho_b + \rho\right)} \tag{23}$$

$$b_p = \frac{3\rho}{2\rho_b + \rho}. \tag{24}$$

2.3. Bubble-particle collision kernel without gravity effect

Eq. (13) is expanded as follows:

$$\begin{aligned}\overline{\mathbf{W}^2} &= \overline{\mathbf{V}_{bI}^2} + \overline{\mathbf{V}_{pI}^2} - \overline{2\mathbf{V}_{pI}\mathbf{V}_{bI}} + R_{bx}^2\overline{\left(\frac{\partial \mathbf{V}_{bI}}{\partial x}\right)^2} + R_{by}^2\overline{\left(\frac{\partial \mathbf{V}_{bI}}{\partial y}\right)^2} + R_{bz}^2\overline{\left(\frac{\partial \mathbf{V}_{bI}}{\partial z}\right)^2} \\ &+ R_{px}^2\overline{\left(\frac{\partial \mathbf{V}_{pI}}{\partial x}\right)^2} + R_{py}^2\overline{\left(\frac{\partial \mathbf{V}_{pI}}{\partial y}\right)^2} + R_{pz}^2\overline{\left(\frac{\partial \mathbf{V}_{pI}}{\partial z}\right)^2} \\ &+ 2\overline{\left(R_{px}R_{bx}\right)\left(\frac{\partial \mathbf{V}_{pI}}{\partial x}\cdot\frac{\partial \mathbf{V}_{bI}}{\partial x}\right)} + 2\overline{\left(R_{py}R_{by}\right)\left(\frac{\partial \mathbf{V}_{pI}}{\partial y}\cdot\frac{\partial \mathbf{V}_{bI}}{\partial y}\right)} + 2\overline{\left(R_{pz}R_{bz}\right)\left(\frac{\partial \mathbf{V}_{pI}}{\partial z}\cdot\frac{\partial \mathbf{V}_{bI}}{\partial z}\right)}\end{aligned} \tag{25}$$

Here the bubble and particle velocity variances and covariance ($\overline{\mathbf{V}_{bI}^2}$, $\overline{\mathbf{V}_{pI}^2}$, and $\overline{\mathbf{V}_{bI}\mathbf{V}_{pI}}$) are determined by

$$\overline{\mathbf{V}_{bI}^2} = A_b\overline{\mathbf{V}^2} \tag{26}$$

$$\overline{\mathbf{V}_{pI}^2} = A_p\overline{\mathbf{V}^2} \tag{27}$$

$$\overline{\mathbf{V}_{bI}\mathbf{V}_{pI}} = B\overline{\mathbf{V}^2} \tag{28}$$

where A_b, A_p, and B are calculated as shown in Appendix. Substitution of Eqs. (26)-(28) into Eq. (25) gives

$$\begin{aligned}\overline{\mathbf{W}^2} &= \left(A_p - 2B + A_b\right)\overline{\mathbf{V}^2} + \left(R_{px}^2\frac{\partial^2}{\partial x^2} + R_{py}^2\frac{\partial^2}{\partial y^2} + R_{pz}^2\frac{\partial^2}{\partial z^2}\right)A_p\overline{\mathbf{V}^2} \\ &+ \left(R_{bx}^2\frac{\partial^2}{\partial x^2} + R_{by}^2\frac{\partial^2}{\partial y^2} + R_{bz}^2\frac{\partial^2}{\partial z^2}\right)A_b\overline{\mathbf{V}^2} + 2B\left(R_{px}R_{bx}\frac{\partial^2}{\partial x^2} + R_{py}R_{by}\frac{\partial^2}{\partial y^2} + R_{pz}R_{bz}\frac{\partial^2}{\partial z^2}\right)\overline{\mathbf{V}^2}\end{aligned} \tag{29}$$

After re-arranging, we have equivalently

$$\overline{\mathbf{W}^2} = \left(A_p - 2B + A_b\right)\overline{\mathbf{V}^2} + \left(R_{px}^2 A_p + 2BR_{px}R_{bx} + R_{bx}^2 A_b\right)\frac{\partial^2 \overline{\mathbf{V}^2}}{\partial x^2}$$
$$+\left(R_{py}^2 A_p + 2BR_{py}R_{by} + R_{by}^2 A_b\right)\frac{\partial^2 \overline{\mathbf{V}^2}}{\partial y^2} + \left(R_{pz}^2 A_p + 2BR_{pz}R_{bz} + R_{bz}^2 A_b\right)\frac{\partial^2 \overline{\mathbf{V}^2}}{\partial z^2} \quad (30)$$

Since the turbulent flow field is isotropic, the following relation holds (Taylor, 1935)

$$\overline{\left(\frac{\partial \mathbf{V}}{\partial x}\right)^2} = \overline{\left(\frac{\partial \mathbf{V}}{\partial y}\right)^2} = \overline{\left(\frac{\partial \mathbf{V}}{\partial z}\right)^2} = \frac{\varepsilon}{3\nu}. \quad (31)$$

Substitution of Eq. (31) into Eq. (30) gives

$$\overline{\mathbf{W}^2} = \underbrace{\left(A_b + A_p - 2B\right)\overline{\mathbf{V}^2}}_{acceleration} + \underbrace{\left(A_b R_b^2 + A_p R_p^2 + 2BR_p R_b\right)\left(\frac{\varepsilon}{3\nu}\right)}_{shear}. \quad (32)$$

In the absence of gravity, we can assume the isotropy of particle and bubble motions and the normal distribution of $\mathbf{V}_p$, $\mathbf{V}_b$, and $\mathbf{W}$, thus

$$\overline{|\mathbf{W}|} = \left(\frac{8\overline{\mathbf{W}^2}}{3\pi}\right)^{1/2}. \quad (33)$$

The bubble-particle collision kernel without gravity effect is determined by

$$\Gamma = \pi R^2 \overline{|\mathbf{W}|}. \quad (34)$$

Substitution of Eqs. (32) and (33) into Eq. (34) yields

$$\Gamma = R^2\left(\frac{8\pi}{3}\right)^{1/2}\left[\left(A_b + A_p - 2B\right)\overline{\mathbf{V}^2} + \left(A_b R_b^2 + A_p R_p^2 + 2BR_p R_b\right)\frac{\varepsilon}{3\nu}\right]^{1/2} \quad (35)$$

If the particles and bubbles have very small inertia ($\tau_p \to 0, \tau_b \to 0$) and follow the fluid completely, we have $A_p \to 1$, $A_b \to 1$ and $B \to 1$. Then, Eq. (35) becomes

$$\Gamma = \left(\frac{8\pi}{9}\right)^{1/2} R^3 \left(\frac{\varepsilon}{\nu}\right)^{1/2} \approx 1.67 R^3 \left(\frac{\varepsilon}{\nu}\right)^{1/2} \tag{36}$$

We refer Eq. (35) and Eq. (36) to as Model 1 and Model 2, respectively. Note that these models are analogically similar to the particle-particle collision models given by Yuu (1984) which are not applicable to the particle-bubble collision interaction in flotation due to the different size scales of (micrometer) solid particles and (millimeter) air bubbles as described below.

For fine particles and small air bubbles in flotation, the correlations of bubble and particle velocities are respectively determined by Nguyen and Schulze (2004) as follows:

$$\sqrt{\overline{V_b^2}} = 0.83 \frac{\varepsilon^{4/9} R_b^{7/9}}{\nu^{1/3}} \left(\frac{\rho - \rho_b}{\rho}\right)^{2/3} \tag{37}$$

$$\sqrt{\overline{V_p^2}} = \frac{2R_p^3}{135} \frac{\varepsilon}{\nu^2} \left(\frac{\rho_p - \rho}{\rho}\right). \tag{38}$$

Equations (37) and (38) were established based on the balance for fine bubbles between the inertial subrange acceleration and Allen's drag, and the balance for fine particles between the dissipative subrange acceleration and Stokes' drag. Note that $\overline{\mathbf{V}_{bI}^2} = 3\overline{V_b^2}$ and $\overline{\mathbf{V}_{pI}^2} = 3\overline{V_p^2}$. Making use of Eqs. (37) and (38) to determine $\overline{\mathbf{V}_{bI}^2}$ and $\overline{\mathbf{V}_{pI}^2}$, Eq. (25) becomes

$$\begin{aligned} \overline{\mathbf{W}^2} = 2.0667 \frac{\varepsilon^{8/9} R_b^{14/9}}{\nu^{2/3}} \left(\frac{\rho - \rho_b}{\rho}\right)^{4/3} + \frac{4R_p^6}{6075} \frac{\varepsilon^2}{\nu^4} \left(\frac{\rho_p - \rho}{\rho}\right)^2 \\ -2B\overline{\mathbf{V}^2} + A_b R_b^2 \frac{\varepsilon}{3\nu} + A_p R_p^2 \frac{\varepsilon}{3\nu} + 2BR_p R_b \frac{\varepsilon}{3\nu} \end{aligned} \tag{39}$$

Substitution of Eq. (39) into Eq. (34) gives

$$\Gamma = R^2 \left(\frac{8\pi}{3}\right)^{1/2} \left[\begin{aligned} &2.0667 \frac{\varepsilon^{8/9} R_b^{14/9}}{\nu^{2/3}} \left(\frac{\rho - \rho_b}{\rho}\right)^{4/3} + \frac{4R_p^6}{6075} \frac{\varepsilon^2}{\nu^4} \left(\frac{\rho_p - \rho}{\rho}\right)^2 \\ &-2B\overline{\mathbf{V}^2} + A_b R_b^2 \frac{\varepsilon}{3\nu} + A_p R_p^2 \frac{\varepsilon}{3\nu} + 2BR_p R_b \frac{\varepsilon}{3\nu} \end{aligned} \right]^{1/2} \tag{40}$$

Equation (40) is our proposed model. The six terms in the square bracket on the RHS of (40)

represent the effect of bubble acceleration, particle acceleration, the coupling of bubble-particle acceleration, bubble shear, particle shear, and bubble-particle shear coupling on the bubble-particle collision kernel, respectively.

2.4. Bubble-particle collision kernel with gravity effect

When the gravitational forces acting on the bubble and particles are considered, we adapt Abrahamson's solution (Abrahamson, 1975) to obtain the bubble-particle relative velocity as follows:

$$\left|\overline{\mathbf{W}'}\right| = \left|V_{pz} + V_{bz}\right| f\left(\frac{\sqrt{\overline{\mathbf{W}^2}/3}}{V_{pz} + V_{bz}}\right) \tag{41}$$

where V_{pz} and V_{bz} are the terminal velocities of particle settling and bubble rising, respectively; erf is the error function, and $\overline{\mathbf{W}^2}$ is determined by Eq. (39). The function in Eq. (41) is defined as follows:

$$f(x) = \frac{2^{3/2}x}{\pi^{1/2}}\exp\left\{-\frac{1}{2x^2}\right\} + \left(1+x^2\right) erf\left\{\frac{1}{\sqrt{2}x}\right\} \tag{42}$$

In the case of no turbulence, Eq. (41) becomes

$$\left|\overline{\mathbf{W}'}\right| = \left|V_{pz} + V_{bz}\right|. \tag{43}$$

In the absence of gravity, Eq. (41) reduces to

$$\left|\overline{\mathbf{W}'}\right| = \left(\frac{8\overline{\mathbf{W}^2}}{3\pi}\right)^{1/2} \tag{44}$$

which is identical to Eq. (33). The bubble-particle collision kernel with gravity effect is determined by

$$\Gamma = \pi R^2 \left|\overline{\mathbf{W}'}\right| \tag{45}$$

3. RESULTS AND DISCUSSION

The integral time scale in isotropic turbulence is given by (Yuu, 1984)

$$T_{fL} = \frac{0.265\overline{\mathbf{V}^2}}{\varepsilon}. \tag{46}$$

In the isotropic turbulence

$$\overline{V_x^2} = \overline{V_y^2} = \overline{V_z^2} = \frac{\overline{\mathbf{V}^2}}{3} = u_0^2 \tag{47}$$

where u_0^2 is the mean square intensity of turbulence. The Lagrangian integral length scale is given by (Abrahamson, 1975)

$$L_L = T_{fL}\sqrt{u_0^2}. \tag{48}$$

3.1. Model verification

Consider $\overline{\mathbf{V}^2} = 0.01\ \mathrm{m^2/s^2}$, $\nu = 1.002\times10^{-6}\ \mathrm{m^2/s}$ (at 20^oC), the liquid density $\rho = 10^3\ \mathrm{kg/m^3}$, the particle density $\rho_p = 1.3\times10^3\ \mathrm{kg/m^3}$ (coal) and $5.0\times10^3\ \mathrm{kg/m^3}$ (sulfide minerals), the bubble density $\rho_b = 1.4\ \mathrm{kg/m^3}$, the gas-liquid surface tension $\sigma = 70\ \mathrm{mN/m}$ and $\varepsilon = 5\ \mathrm{W/kg}$. We obtain $T_{fL} = 5.3\times10^{-4}\ \mathrm{s}$ and $L_L = 31\ \mu\mathrm{m}$. The minimum and maximum limits of particle radius R_p are chosen to be $5\mu\mathrm{m}$ and $250\mu\mathrm{m}$, respectively. Figs. 2a and 2b present the result of bubble-particle collision kernel with respect to (w.r.t.) R_p for $\rho_p = 1.3\times10^3\ \mathrm{kg/m^3}$ and $5.0\times10^3\ \mathrm{kg/m^3}$, respectively. The present results are compared with those of other models including Models 1 and 2, Bloom and Heindel (2002)'s model and Nguyen and Schulze (2004)'s model. Nguyen and Schulze's model is as follows:

$$\Gamma = \pi R^2 \left(V_{pz} + V_{bz}\right) f\left[\frac{\sqrt{\overline{V_b^2} + \overline{V_p^2}}}{V_{pz} + V_{bz}}\right] \tag{49}$$

where Eq. (42) describes the function *f*, the bubble and particle velocity variances, $\overline{V_b^2}$ and $\overline{V_p^2}$, are determined by Eqs. (37) and (38), respectively. It can be seen that for $\rho_p = 1.3\times10^3\ \mathrm{kg/m^3}$ the

present model agrees well with Model 1 and yields larger values of collision kernel than Model 2, Bloom and Heindel's model, and Nguyen and Schulze's model. Note that for small particle and bubble inertias (viscous subrange) in a water flow, the spatial variation of turbulence (shear effect) is the predominant factor in the collision process. However, for the particles and bubbles with larger inertia (inertial subrange) their relative motion to the water becomes important, which results in a higher collision kernel. As expected, the present model and Model 1 produce higher collision kernel than Model 2 and Nguyen and Schulze's model.

For heavier particles, $\rho_p = 5.0\times10^3$ kg/m^3, a similar behavior is obtained for small particle sizes ($R_p < 100\mu$m), however, for larger particles ($R_p > 200\mu$m) the particle acceleration becomes larger, the velocity pulsations of particle and bubble are statistically independent and the shear effect becomes negligible. Therefore, the present model yields almost the same results as Nguyen and Schulze's model. Note that Nguyen and Schulze's model was developed based on Abrahamson's model. In their model, the bubble and particle velocity variances are determined through the balance for fine bubbles between the inertial subrange acceleration and Allen's drag and the balance for fine particles between the dissipative subrange acceleration and Stokes' drag, respectively. Figs. 3a and 3b show the bubble-particle collision kernels of the present model with and without gravity effect in comparison with those of Model 1 and Nguyen and Schulze (2004)'s model for $\rho_p = 1.3\times10^3$ kg/m^3 and $\rho_p = 5.0\times10^3$ kg/m^3, respectively. It appears that all the models yield higher collision coefficients when the gravity effect is added.

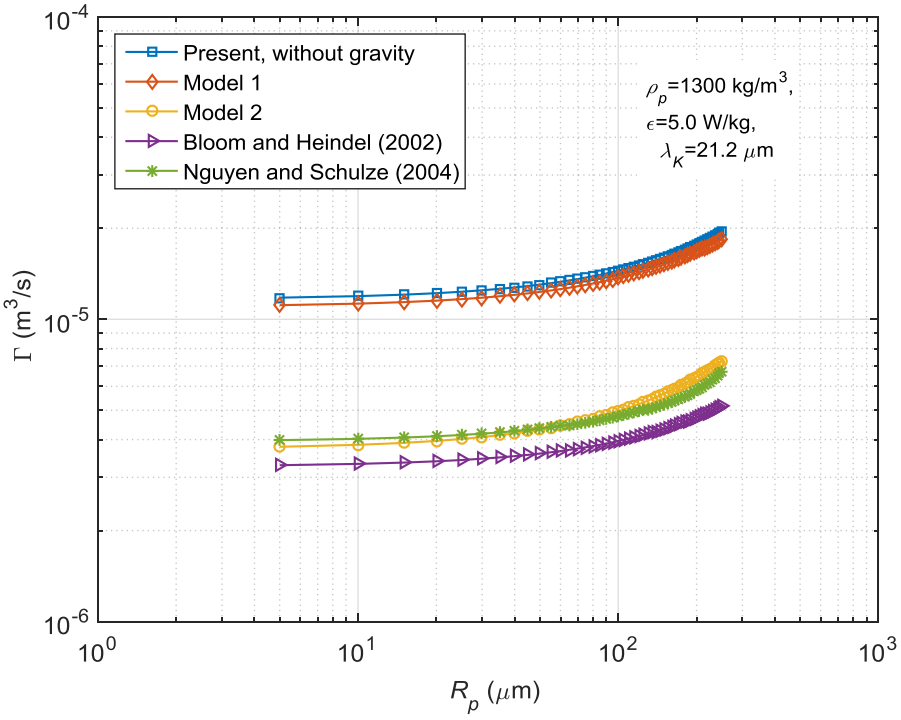

(a)

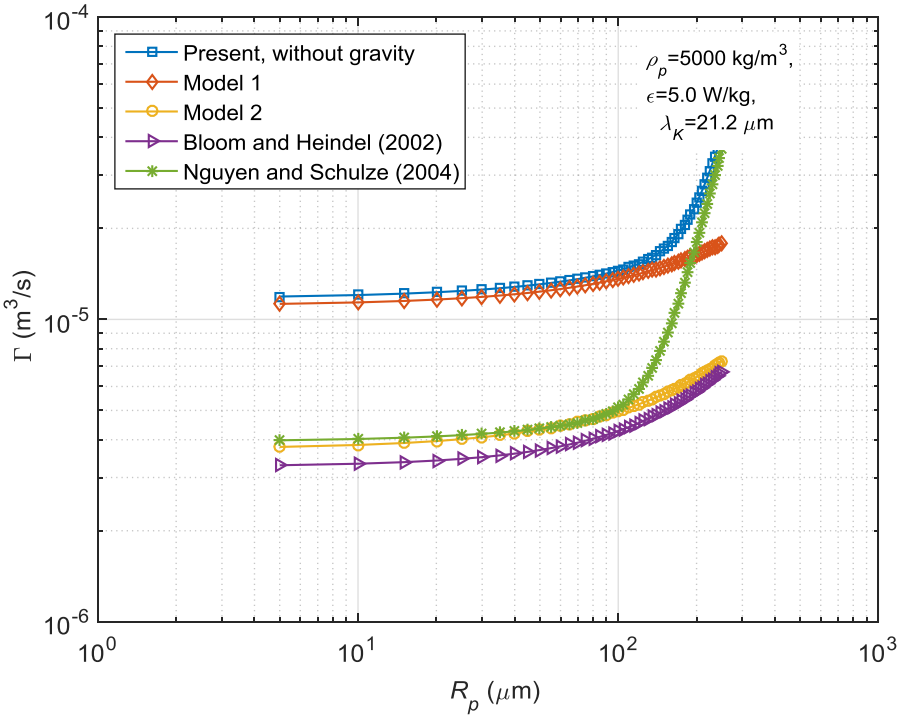

(b)

Figure 2. Comparison of bubble-particle collision kernel among different models, neglecting the gravity effect, for $R_b = 1.0$ mm, $\varepsilon = 5$ W/kg, (a) $\rho_p = 1.3\times10^3$ kg/m^3, and (b) 5.0×10^3 kg/m^3.

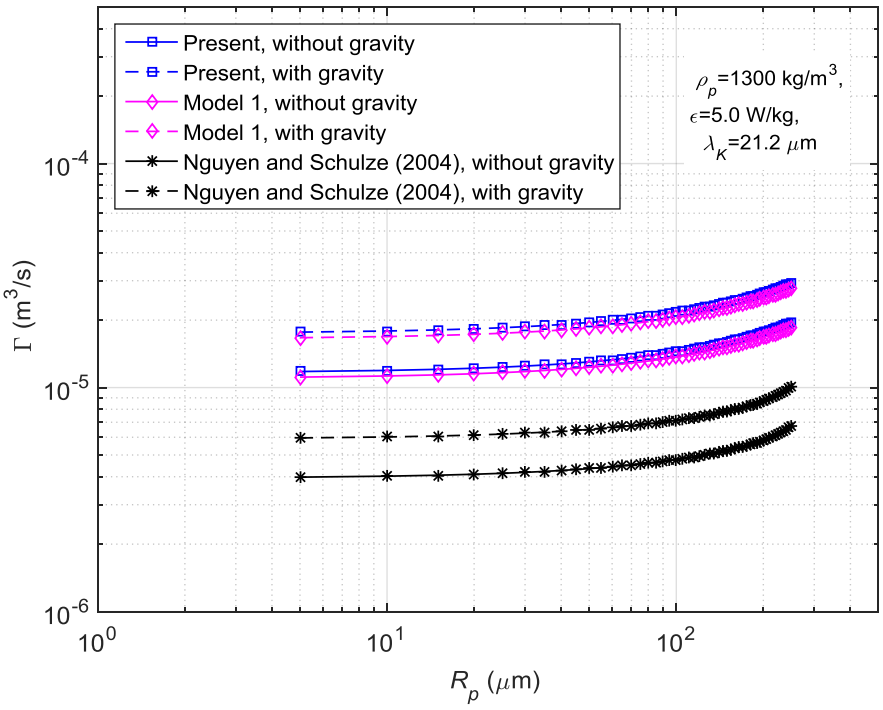

(a)

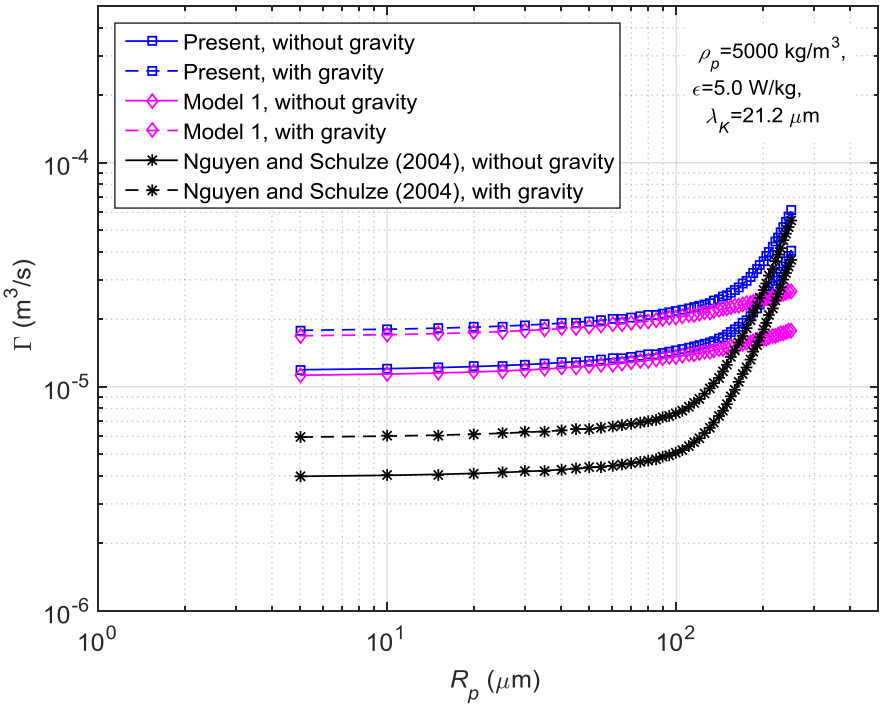

(b)

Figure 3. Comparison of bubble-particle collision kernel among different models, with and without gravity effect, for $R_b = 1.0\,\text{mm}$, $\varepsilon = 5\,\text{W/kg}$, (a) $\rho_p = 1.3\times10^3\,\text{kg/m}^3$, and (b) $5.0\times10^3\,\text{kg/m}^3$.

3.2. Influence of shear, acceleration and gravity effects on collision kernel

Eq. (39) can be written as

$$\overline{\mathbf{W}^2} = \overline{\mathbf{W}_{ba}^2} + \overline{\mathbf{W}_{pa}^2} + \overline{\mathbf{W}_{bpa}^2} + \overline{\mathbf{W}_{bs}^2} + \overline{\mathbf{W}_{ps}^2} + \overline{\mathbf{W}_{bps}^2} \tag{50}$$

where the subscripts *ba*, *pa*, *bpa*, *bs*, *ps*, and *bps* represent the effects of bubble acceleration, particle acceleration, bubble-particle acceleration coupling, bubble shear, particle shear, and bubble-particle shear coupling, respectively.

In order to investigate the effects of shear, acceleration, and gravity on the collision kernel, we determine the following collision coefficients based on the combination of different effects.

$$\Gamma_{ba} = R^2 \left(\frac{8\pi}{3}\right)^{1/2} \left[\overline{\mathbf{W}_{ba}^2}\right]^{1/2}, \tag{51}$$

$$\Gamma_{ba+pa} = R^2 \left(\frac{8\pi}{3}\right)^{1/2} \left[\overline{\mathbf{W}_{ba}^2} + \overline{\mathbf{W}_{pa}^2}\right]^{1/2}, \tag{52}$$

$$\Gamma_{ba+pa+bpa} = R^2 \left(\frac{8\pi}{3}\right)^{1/2} \left[\overline{\mathbf{W}_{ba}^2} + \overline{\mathbf{W}_{pa}^2} + \overline{\mathbf{W}_{bpa}^2}\right]^{1/2}, \tag{53}$$

$$\Gamma_{ba+pa+bpa+bs} = R^2 \left(\frac{8\pi}{3}\right)^{1/2} \left[\overline{\mathbf{W}_{ba}^2} + \overline{\mathbf{W}_{pa}^2} + \overline{\mathbf{W}_{bpa}^2} + \overline{\mathbf{W}_{bs}^2}\right]^{1/2}, \tag{54}$$

$$\Gamma_{ba+pa+bpa+bs+ps} = R^2 \left(\frac{8\pi}{3}\right)^{1/2} \left[\overline{\mathbf{W}_{ba}^2} + \overline{\mathbf{W}_{pa}^2} + \overline{\mathbf{W}_{bpa}^2} + \overline{\mathbf{W}_{bs}^2} + \overline{\mathbf{W}_{ps}^2}\right]^{1/2}, \tag{55}$$

$$\Gamma_{ba+pa+bpa+bs+ps+bps} = R^2 \left(\frac{8\pi}{3}\right)^{1/2} \left[\overline{\mathbf{W}_{ba}^2} + \overline{\mathbf{W}_{pa}^2} + \overline{\mathbf{W}_{bpa}^2} + \overline{\mathbf{W}_{bs}^2} + \overline{\mathbf{W}_{ps}^2} + \overline{\mathbf{W}_{bps}^2}\right]^{1/2}, \tag{56}$$

$$\Gamma_{ba+pa+bpa+bs+ps+bps+g} = \pi R^2 \overline{\left|\mathbf{W}'\right|}, \tag{57}$$

$$\Gamma_a = \Gamma_{ba+pa+bpa}, \tag{58}$$

$$\Gamma_s = \Gamma_{ba+pa+bpa+bs+ps+bps} - \Gamma_{ba+pa+bpa}, \tag{59}$$

$$\Gamma_g = \Gamma_{ba+pa+bpa+bs+ps+bps+g} - \Gamma_{ba+pa+bpa+bs+ps+bps}, \quad (60)$$

where the subscripts *a*, *s*, and *g* represent the effects of acceleration, shear, and gravity, respectively.

The variation of the Γ_a / Γ_g and Γ_s / Γ_g ratios w.r.t. R_p is given in Figs. 4a and 4b for $\rho_p = 1.3\times10^3$ kg/m^3 and $\rho_p = 5.0\times10^3$ kg/m^3, respectively. For $\rho_p = 1.3\times10^3$ kg/m^3, the shear effect is the dominant factor for the whole range of particle sizes $5\mu\text{m} \le R_p \le 250\mu\text{m}$. For the heavier particles $\rho_p = 5.0\times10^3$ kg/m^3, the shear effect is dominant and larger than the gravity effect and the gravity effect is larger than the acceleration effect for $R_p < 7.32\lambda_K$; however, for $R_p > 7.32\lambda_K$ the acceleration effect is dominant and larger than the gravity effect, and the gravity effect is larger than the shear effect.

Figs. 5a and 5b show the effects of bubble acceleration, particle acceleration, bubble-particle acceleration coupling, bubble shear, particle shear, bubble-particle shear coupling and gravity on the bubble-particle collision kernel for $\rho_p = 1.3\times10^3$ kg/m^3 and $\rho_p = 5.0\times10^3$ kg/m^3, respectively. For $\rho_p = 5.0\times10^3$ kg/m^3, the obtained results indicate that the shear effect plays an important role in small particle sizes while the acceleration effect becomes dominant for large particle sizes. The bubble shear effect is much larger than the particle shear effect because the bubble is bigger and lighter than the particle. The bubble-particle shear coupling effect is quite small. The bubble-particle acceleration coupling effect slightly reduces the collision kernel. The gravity effect increases the collision kernel for all particle length scales, and the acceleration effect is dominant for large particle inertias.

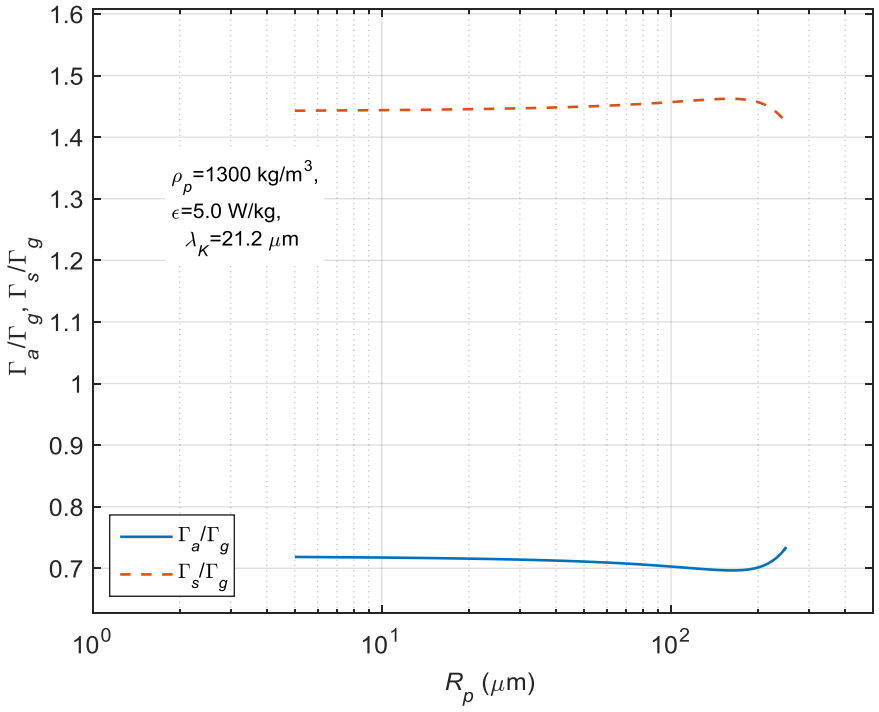

(a)

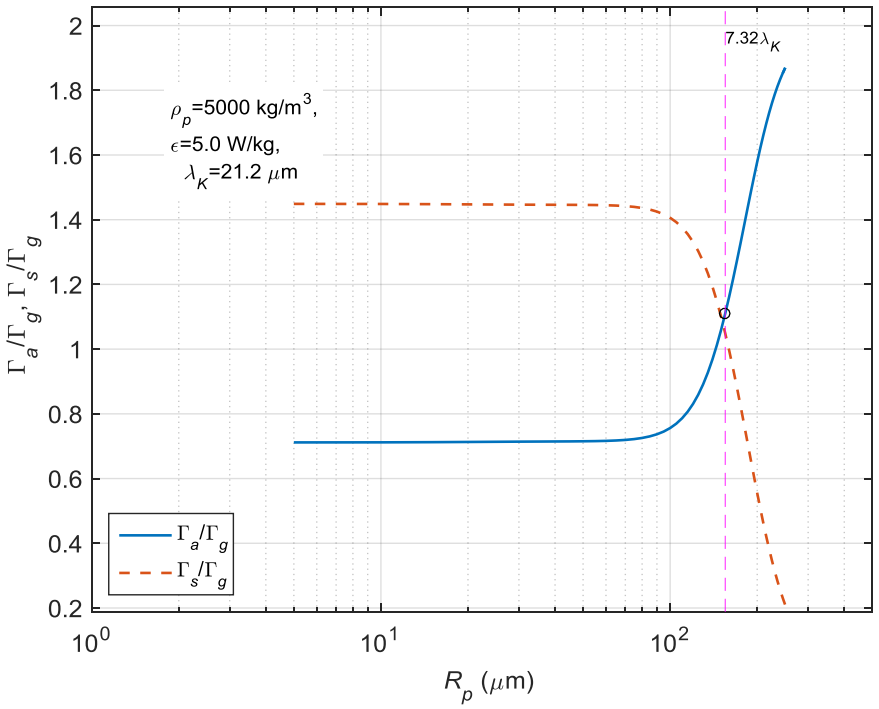

(b)

Figure 4. Bubble-particle collision: the ratios of acceleration effect and shear effect to gravity effect, for $R_b = 1.0\text{mm}$, $\varepsilon = 5\,\text{W/kg}$, (a) $\rho_p = 1.3\times10^3\ \text{kg/m}^3$, and (b) $5.0\times10^3\ \text{kg/m}^3$.

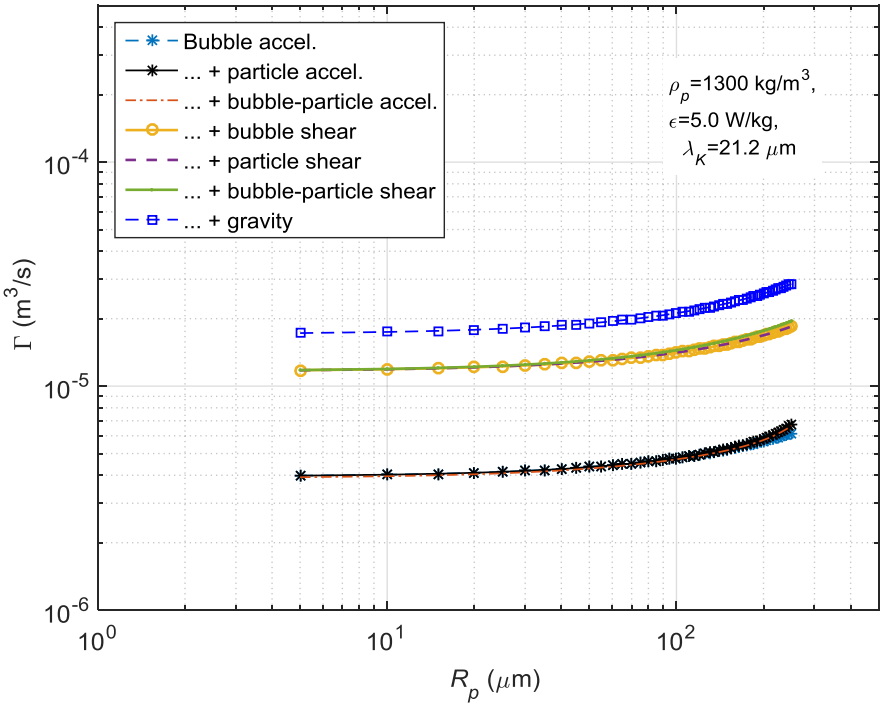

(a)

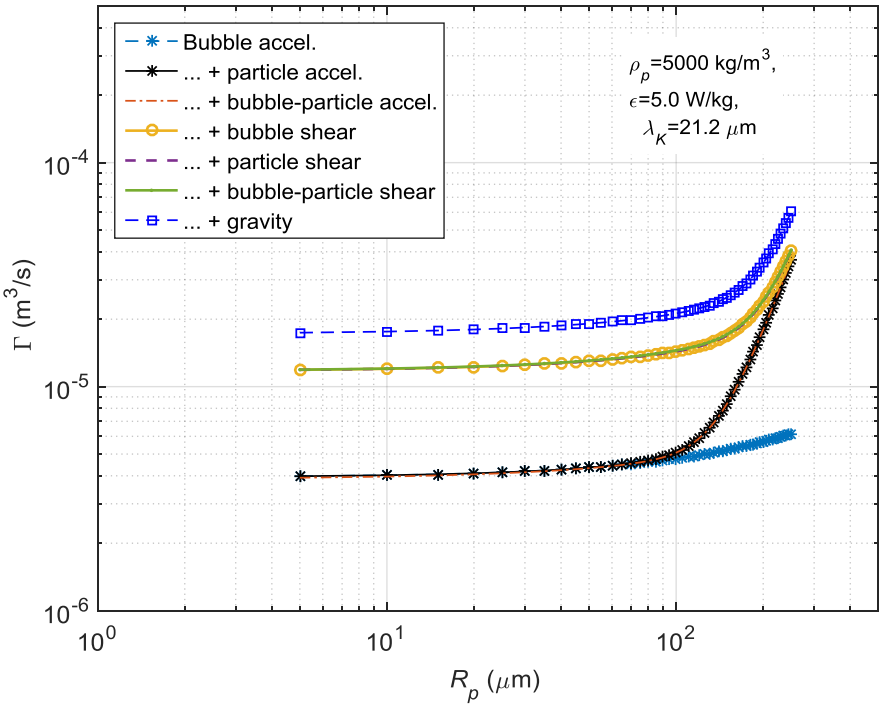

(b)

Figure 5. Bubble-particle collision: effects of bubble acceleration, particle acceleration, bubble-particle acceleration coupling, bubble shear, particle shear, bubble-particle shear coupling and

gravity on the bubble-particle collision kernel, (a) $\rho_p = 1.3\times10^3$ kg/m^3, and (b) 5.0×10^3 kg/m^3.

3.3. *Influence of R_b, R_p, ε and ρ_p on collision kernel and efficiency*

Figs. 6a and 6b present the bubble-particle collision kernel (Γ) and efficiency (E_c) w.r.t. R_p for $\rho_p = 2\times10^3$ kg/m^3, $\varepsilon = 5$ W/kg and different values of $R_b = \{0.5, 1.0, 2.0\}$ mm, while the corresponding results for $\rho_p = 2\times10^3$ kg/m^3, $R_b = 1$ mm and different values of $\varepsilon = \{1, 2, 5\}$ W/kg are given in Figs. 7a and 7b, respectively. Figs. 8a and 8b provide the bubble-particle collision kernel and efficiency w.r.t. ε for $\rho_p = 2\times10^3$ kg/m^3, $R_b = 1$ mm and different values of $R_p = \{50, 150, 250\}$ μm. It can be seen that the collision kernel increases with increasing particle and bubble sizes, and dissipation rate of turbulent kinetic energy (Figs. 6a, 7a, 8a). It is noted that turbulence can significantly enhance the relative motion between the bubble and particles. The relative motion can be faster than the relative counter-current motion between the bubble rise and particle settling. As a result, $E_c > 1$ if $\varepsilon > 0$ and $E_c = 1$ if $\varepsilon = 0$. Fig. 6b indicates that the variation in particle size does not affect the collision efficiency significantly for $R_b = 0.5$ and 1.0 mm. For larger bubble size $R_b = 2.0$ mm, the collision efficiency reduces as the particle size increases, although the collision kernel increases with increasing particle size as shown in Fig. 6a because the gravitational force acting on the bubble is dominant. For a given value of ε, E_c tends to reduce with increasing R_p (Fig. 7b). Fig. 8 shows that the collision kernel and efficiency are intensified as the turbulence dissipation rate increases, for all values of R_p. Figs. 9a and 9b show the bubble-particle collision kernel and efficiency w.r.t. R_p for $R_b = 1.0$ mm, $\varepsilon = 5$ W/kg and different values of $\rho_p = \{1.3, 2.0, 5.0\}\times10^3$ kg/m^3. It appears that Γ and E_c increase with increasing ρ_p for large particle sizes ($R_p < 150$ μm) while Γ and E_c are almost unchanged w.r.t. ρ_p for small particle sizes ($R_p > 150$ μm).

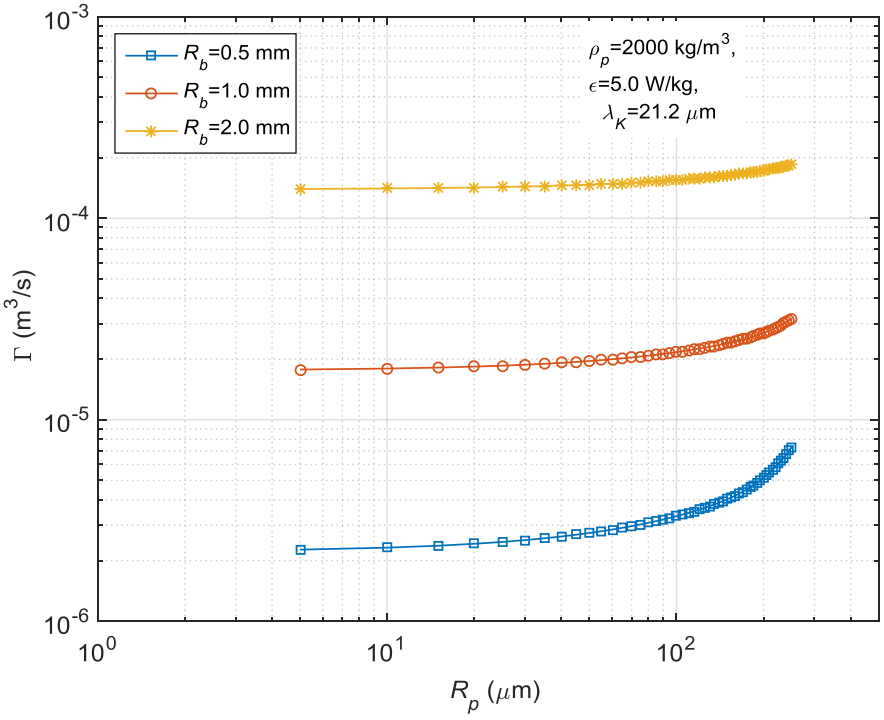

(a)

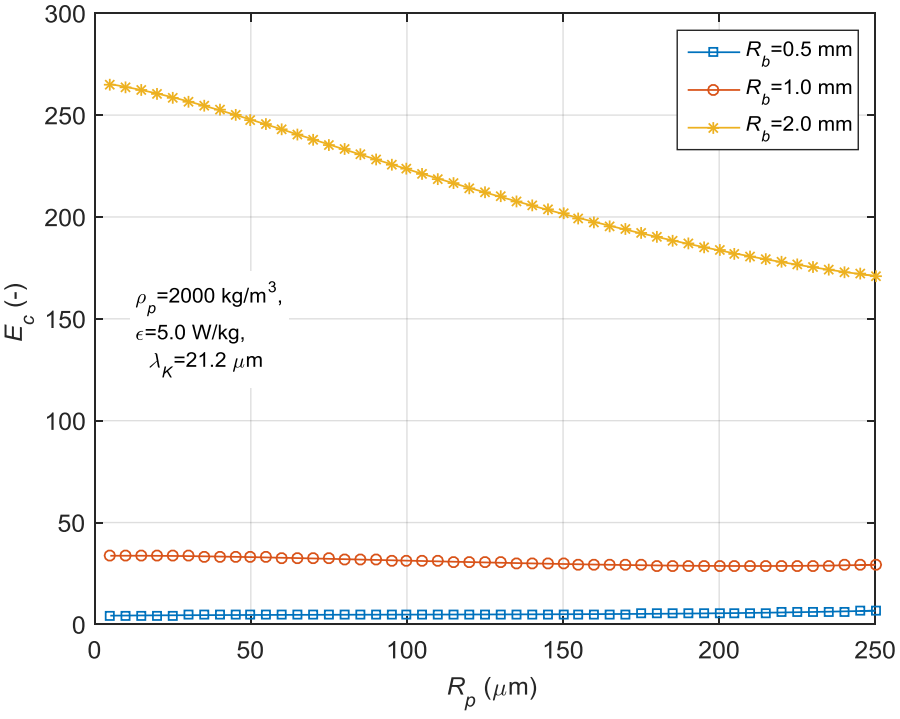

(b)

Figure 6. (a) Bubble-particle collision kernel and (b) collision efficiency w.r.t. R_p for $\rho_p = 2\times10^3$ kg/m^3, $\varepsilon = 5$ W/kg and different values of $R_b = \{0.5, 1.0, 2.0\}$ mm.

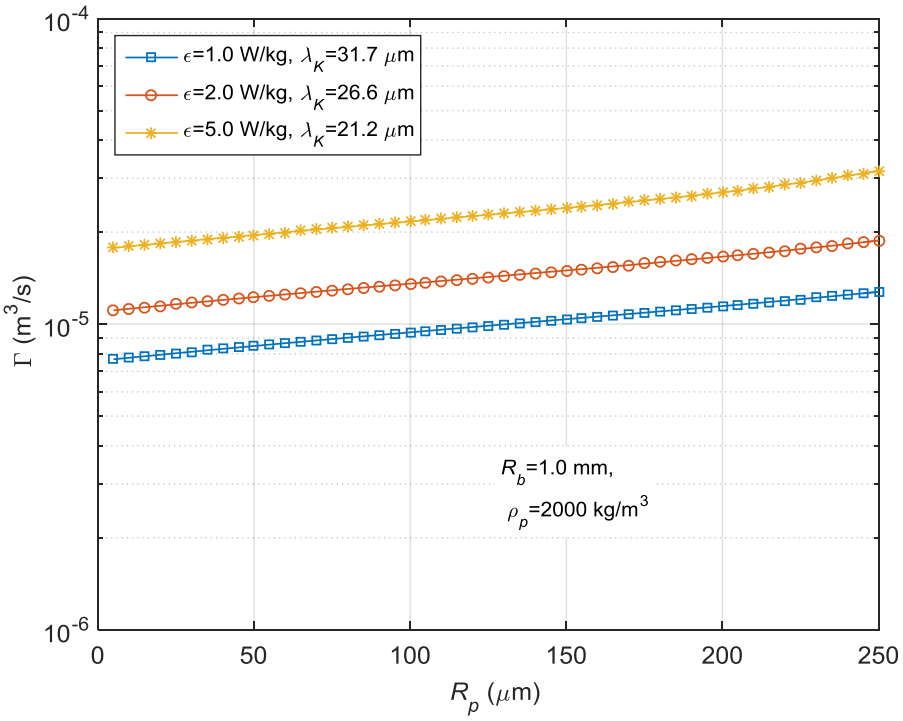

(a)

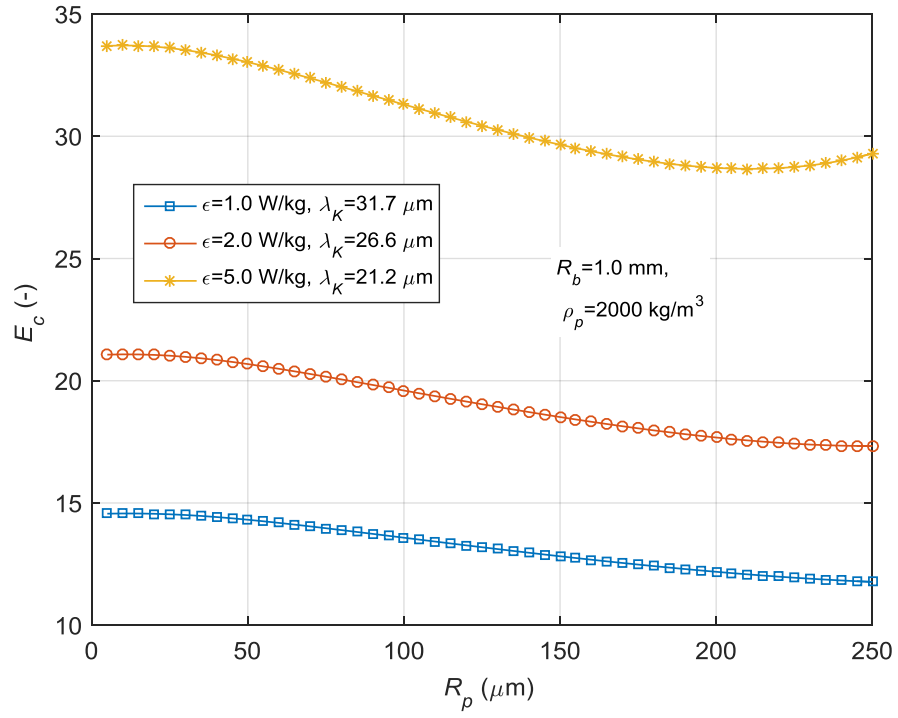

(b)

Figure 7. (a) Bubble-particle collision kernel and (b) collision efficiency w.r.t. R_p for $\rho_p = 2\times10^3$ kg/m^3, $R_b = 1$ mm and different values of $\varepsilon = \{1, 2, 5\}$ W/kg.

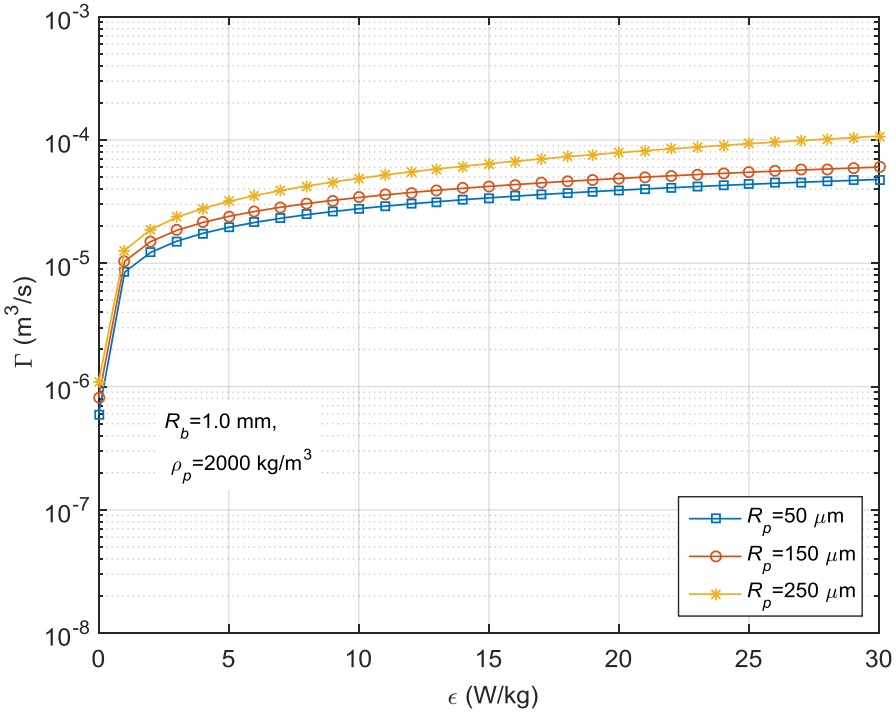

(a)

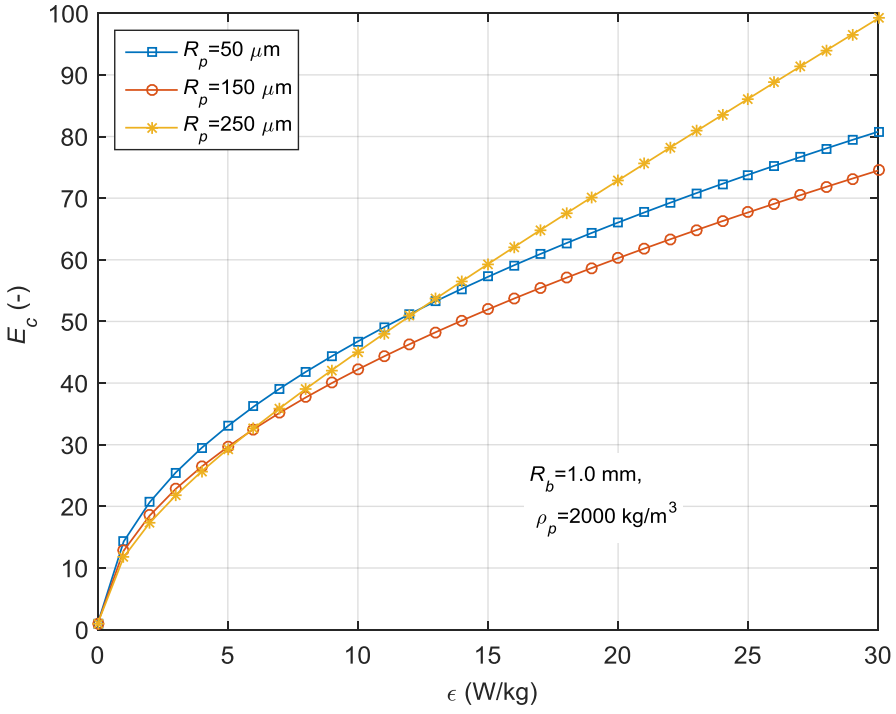

(b)

Figure 8. (a) Bubble-particle collision kernel and (b) collision efficiency w.r.t. ε for $\rho_p = 2\times10^3$ kg/m^3, $R_b = 1mm$ and different values of $R_p = \{50, 150, 250\}$ μm.

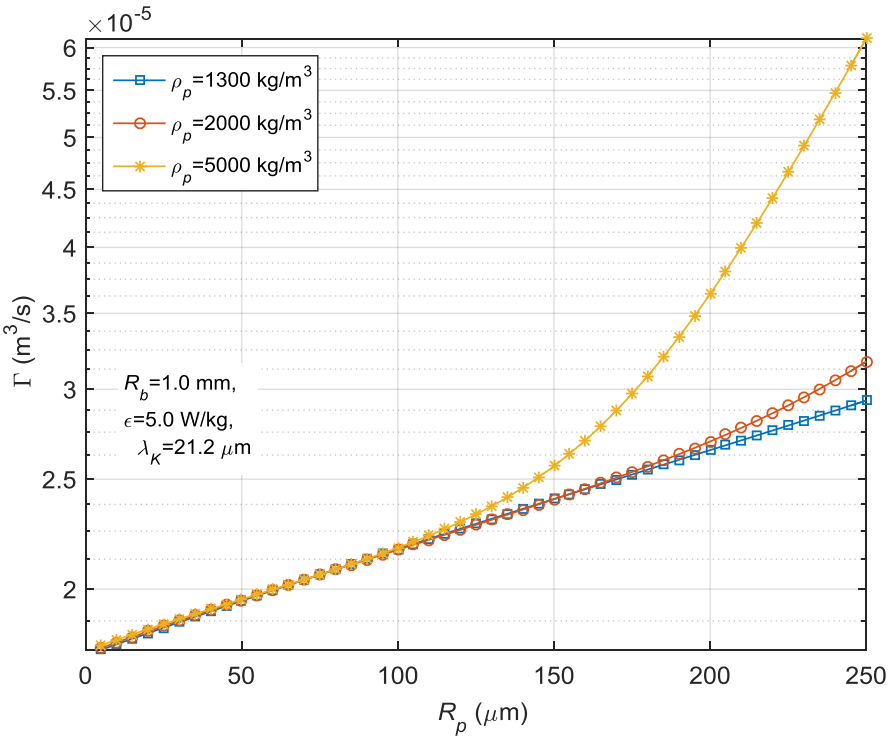

(a)

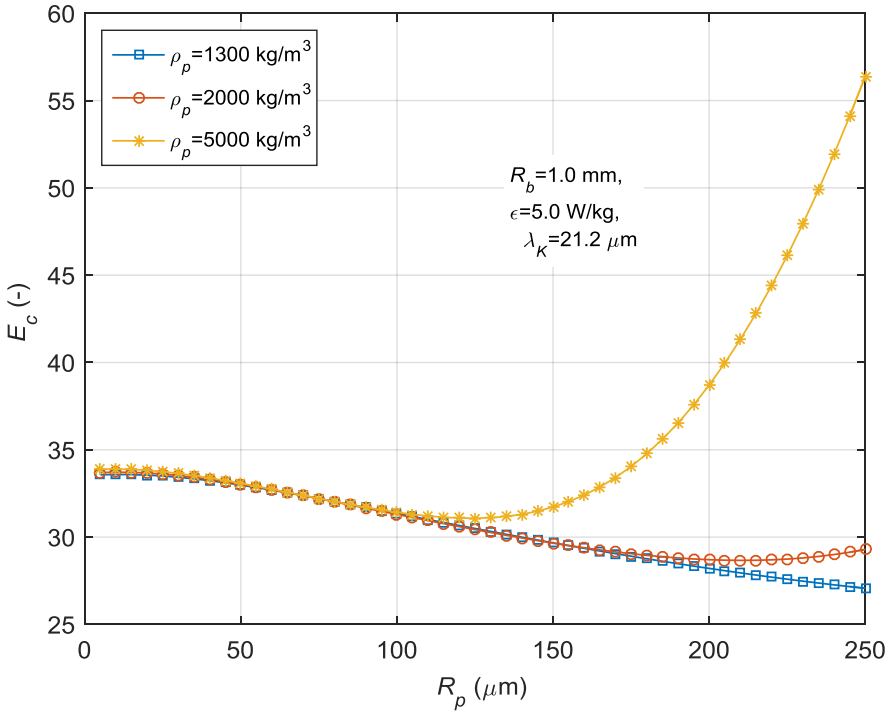

(b)

Figure 9. (a) Bubble-particle collision kernel and (b) collision efficiency w.r.t. R_p for $R_b = 1.0$ mm, $\varepsilon = 5$ W/kg and different values of $\rho_p = \{1.3, 2.0, 5.0\} \times 10^3$ kg/m^3.

4. CONCLUSIONS

In this paper, we have developed a theoretical model of bubble-particle collision in the homogeneous and isotropic turbulence flow, taking into account the effects of acceleration, shear, and gravity of the bubble-particle system. The bubble and particle velocity variances are calculated by using Nguyen and Schulze's model, while the bubble-particle velocity covariance is determined based on the Basset-Boussinesq-Ossen equation and the correlation method. We use Stokes' law with a particle size correction factor to calculate the drag force acting on a particle and Allen's law to calculate the drag force acting on a bubble. The present model agrees well with Model 1 for small-inertia particles and agrees well with Nguyen and Schulze's model for large-inertia particles. For low-density particles ($\rho_p = 1.3\times10^3$ kg/m^3), the shear effect is always larger than the acceleration effect in the range of $5\,\mu\text{m} \le R_p \le 250\,\mu\text{m}$. However, for heavier particles ($\rho_p = 5.0\times10^3$ kg/m^3), the shear effect is larger than the gravity effect and the gravity effect is larger than the acceleration effect for small particle sizes ($R_p < 7.32\lambda_K$). For large particle sizes ($R_p > 7.32\lambda_K$) the acceleration effect is larger than the gravity effect, and the gravity effect is larger than the shear effect, for the case of $R_b = 1.0$ mm, $\varepsilon = 5$ W/kg, and $\rho_p = 5.0\times10^3$ kg/m^3. The particle shear effect is much smaller than the bubble shear effect because the bubble is bigger and lighter than the particle. The bubble-particle acceleration coupling effect slightly reduces the collision kernel while the bubble-particle shear slightly increases the collision kernel. The bubble-particle collision kernel increases with increasing bubble and particle sizes, and dissipation rate of turbulent kinetic energy. Turbulence intensity enhances the bubble-particle collision kernel and frequency. For given values of ε and R_b, the collision kernel and frequency increase with increasing particle density for large particle sizes and remains unchanged for small particle sizes. The numerical data show that turbulence can increase the collision efficiency, exceeding the ideal rate of collision by gravity and leading to the turbulence collision efficiency greater than unity. Therefore, the collision efficiency due to turbulence cannot be ignored in predicting the overall bubble-particle collision efficiency in flotation.

ACKNOWLEDGEMENTS

This research is supported by Australian Research Council's Project Funding Scheme (Project number DP150100395).

APPENDIX A: BUBBLE AND PARTICLE VELOCITY VARIANCES AND COVARIANCE

The turbulent velocities of fluid, bubble and particle are expressed by using the Fourier integral as follows:

$$V_i(t) = 2\pi\int_0^\infty \left[\alpha_i(M)\cos(2\pi Mt) + \beta_i(M)\sin(2\pi Mt)\right]dM \tag{A.1}$$

$$V_{bIi}(t) = 2\pi\int_0^\infty \left[\gamma_{bi}(M)\cos(2\pi Mt) + \delta_{bi}(M)\sin(2\pi Mt)\right]dM \tag{A.2}$$

$$V_{pIi}(t) = 2\pi\int_0^\infty \left[\gamma_{pi}(M)\cos(2\pi Mt) + \delta_{pi}(M)\sin(2\pi Mt)\right]dM\ . \tag{A.3}$$

Substitution of Eqs. (A.1)-(A.3) into Eqs. (19) and (22) gives

$$\gamma_{bi} = \left[1 + \frac{\omega^2(b_b - 1)}{a_b^2 + \omega^2}\right]\alpha_i + \frac{a_b\omega(b_b - 1)}{a_b^2 + \omega^2}\beta_i \tag{A.4}$$

$$\gamma_{pi} = \left[1 + \frac{\omega^2(b_p - 1)}{a_p^2 + \omega^2}\right]\alpha_i + \frac{a_2\omega(b_p - 1)}{a_p^2 + \omega^2}\beta_i \tag{A.5}$$

$$\delta_{bi} = -\left[\frac{a_b\omega(b_b - 1)}{a_b^2 + \omega^2}\right]\alpha_i + \left[1 + \frac{\omega^2(b_b - 1)}{a_b^2 + \omega^2}\right]\beta_i \tag{A.6}$$

$$\delta_{pi} = -\left[\frac{a_p\omega(b_p - 1)}{a_p^2 + \omega^2}\right]\alpha_i + \left[1 + \frac{\omega^2(b_p - 1)}{a_p^2 + \omega^2}\right]\beta_i\ . \tag{A.7}$$

where $\omega = 2\pi M$.

The correlation $\overline{V_{bIi}(\tau)V_{pIi}(\tau - t)}$ is determined as follows:

$$\overline{V_{bIi}(\tau)V_{pIi}(\tau - t)} = \frac{1}{2T - t}\int_{-T_1}^{T} V_{bIi}(\tau)V_{pIi}(\tau - t)\,d\tau \tag{A.8}$$

where $T_1 > T$. Substituting Eqs. (A.2) and (A.3) into Eq. (A.8), the term $\overline{V_{bIi}(\tau)V_{pIi}(\tau)}$ is computed as

$$\overline{V_{bIi}(\tau)V_{pIi}(\tau)} = \int_0^\infty E_{L_{bpi}}(M)\,dM \tag{A.9}$$

$$E_{L_{bpi}}(M) = \frac{\pi^2}{T}\left[\gamma_{bi}(M)\gamma_{pi}(M) + \delta_{bi}(M)\delta_{pi}(M)\right]. \tag{A.10}$$

Similarly, we obtain

$$\overline{V_i^2(\tau)} = \int_0^\infty E_{fL_i}(M)\,dM \tag{A.11}$$

where

$$E_{fL_i}(M) = \frac{\pi^2}{T}\left[\alpha_i^2(M) + \beta_i^2(M)\right]. \tag{A.12}$$

From Eqs. (A.10) and (A.12), we get

$$E_{L_{bpi}}(M) = \frac{\gamma_{bi}(M)\gamma_{pi}(M) + \delta_{bi}(M)\delta_{pi}(M)}{\alpha_i^2(M) + \beta_i^2(M)} E_{fL_i}(M). \tag{A.13}$$

Hinze (1975) derived the following relation

$$E_{fLi}(M) = 4\overline{V_i^2}\,\frac{T_{fLi}}{1+\omega^2 T_{fLi}^2}. \tag{A.14}$$

Making use of Eqs. (A.10)-(A.14), Eq. (A.9) becomes

$$\overline{V_{bIi}(\tau)V_{pIi}(\tau)} = B\overline{V_i^2} \tag{A.15}$$

where

$$B = \frac{2}{\pi} T_{fLi}\int_0^\infty \left[\frac{\left(a_b^2 + b_b\omega^2\right)\left(a_p^2 + b_p\omega^2\right) + a_b a_p \omega^2 (b_b - 1)(b_p - 1)}{\left(a_b^2 + \omega^2\right)\left(a_p^2 + \omega^2\right)\left(1 + \omega^2 T_{fL}^2\right)}\right] d\omega \tag{A.16}$$

Simplifying Eq. (A.16) gives

$$B = \frac{2}{\pi} T_{fL} \int_0^\infty \left[\frac{k_1}{\left(a_b^2 + \omega^2\right)} + \frac{k_2}{\left(a_p^2 + \omega^2\right)} + \frac{k_3}{\left(1 + \omega^2 T_{fL}^2\right)} \right] d\omega \qquad \text{(A.17)}$$

where $T_{fLi} = T_{fL}$ since the flow field is assumed to be isotropic. The constants are described as follows:

$$k_1 = \frac{a_b^2 a_p - a_b^2 a_p b_b + a_b^3 b_p - a_b^3 b_b b_p}{\left(a_b + a_p\right)\left(1 - a_b^2 T_{fL}^2\right)} \qquad \text{(A.18)}$$

$$k_2 = \frac{a_b a_p^2 + a_p^3 b_b - a_p^2 a_b b_p - a_p^3 b_b b_p}{\left(a_b + a_p\right)\left(1 - a_p^2 T_{fL}^2\right)} \qquad \text{(A.19)}$$

$$k_3 = \frac{b_b b_p - a_b a_p T_{fL}^2 + a_b a_p b_b T_{fL}^2 - a_p^2 b_b T_{fL}^2 - a_b^2 b_p T_{fL}^2 + a_b a_p b_p T_{fL}^2 - a_b a_p b_b b_p T_{fL}^2 + a_b^2 a_p^2 T_{fL}^4}{\left(1 - a_b^2 T_{fL}^2\right)\left(1 - a_p^2 T_{fL}^2\right)}. \qquad \text{(A.20)}$$

Calculating the integral in Eq. (A.17), we obtain

$$B = 1 + \frac{1}{a_b + a_p} \left[\frac{\left(-1 + b_b\right)\left(a_p + a_b b_p\right)}{1 + a_b T_{fL}} + \frac{\left(-1 + b_p\right)\left(a_b + a_p b_b\right)}{1 + a_p T_{fL}} \right]. \qquad \text{(A.21)}$$

Hinze (1975) obtained the following relation between the turbulent intensities of particle and fluid

$$\overline{V_{pIi}^2} = A_p \overline{V_i^2} \qquad \text{(A.22)}$$

where

$$A_p = \frac{a_p T_{fL} + b_p^2}{a_p T_{fL} + 1}. \qquad \text{(A.23)}$$

Similarly, we obtain

$$\overline{V_{bIi}^2} = A_b \overline{V_i^2} \qquad \text{(A.24)}$$

where

$$A_b = \frac{a_b T_{fL} + b_b^2}{a_b T_{fL} + 1}. \tag{A.25}$$

Finally, combining Eqs. (A.15), (A.22), and (A.24), we obtain

$$\overline{\mathbf{V}_{bI}^2} = A_b \overline{\mathbf{V}^2}. \tag{A.26}$$

$$\overline{\mathbf{V}_{pI}^2} = A_p \overline{\mathbf{V}^2} \tag{A.27}$$

$$\overline{\mathbf{V}_{bI}\mathbf{V}_{pI}} = B\overline{\mathbf{V}^2} \tag{A.28}$$

NOMENCLATURE

Small alphabet letters

a	Numerical constant in Eq. (8)
a_b	A factor defined by Eq. (23)
a_p	A factor defined by Eq. (17)
b	Numerical constant in Eq. (8)
b_b	A factor defined by Eq. (24)
b_p	A factor defined by Eq. (18)
d_b	Bubble diameter
d_p	Particle diameter
f_b	Bubble size correction factor
f_p	Particle size correction factor
g	Gravitational acceleration
k	Numerical constant in Eq. (8)
n_b	Bubble number concentration
n_p	Particle number concentration
t	Time
u_0^2	Mean square intensity of turbulence

Capitalized alphabet letters

Ar	Particle Archimedes number
Ar_*	Bubble Archimedes number
E_c	Collision efficiency
$\mathbf{F}_{Db}$	Drag force acting on a bubble
$\mathbf{F}_{Dp}$	Drag force acting on a particle
$\mathbf{J}$	Particle flux vector
L_L	Lagrangian integral length scale
M	Frequency

Mo	Morton number
N_c	Rate of bubble-particle collision
N_{ci}	Ideal rate of bubble-particle collision
R	The sum of bubble and particle radii
R_b	Bubble radius
R_p	Particle radius
Re_b	Bubble Reynolds number
Re_p	Particle Reynolds number
T_{fL}	Lagrangian integral time scale
$\mathbf{V}$	Fluid velocity
$\mathbf{V}_b$	Bubble velocity
$\mathbf{V}_p$	Particle velocity
V_{bz}	Terminal velocity of bubble rising
V_{pz}	Terminal velocity of particle settling
V_K	Kolmogorov velocity scale
$\mathbf{W}$	Bubble-particle relative velocity vector

Greek letters

Γ	Bubble-particle collision kernel
ε	Turbulence dissipation rate
λ_K	Kolmogorov length scale
μ	Dynamic viscosity of a fluid
ν	Kinematic viscosity of a fluid
ρ	Fluid density
ρ_b	Bubble density
ρ_p	Particle density
σ	Surface tension of gas-liquid interface
τ_K	Kolmogorov time scale
ω	Angular frequency

REFERENCES

Abrahamson, J., Collision rates of small particles in a vigorously turbulent fluid. Chemical Engineering Science, 1975, **30**, 1371-1379.

Alipchenkov, V.M., Zaichik, L.I., Particle clustering in isotropic turbulent flow. Fluid Dynamics, 2003, **38(3)**, 417-432.

Ayala, O., Rosa, B., Wang, L.-P., Effects of turbulence on the geometric collision rate of sedimenting droplets. Part 2. Theory and parameterization. New Journal of Physics, 2008, **10**, 075016.

Bloom, F., Heindel, T.J., On the structure of collision and detachment frequencies in flotation models. Chemical Engineering Science, 2002, **57**, 2467-2473.

Dai, Z., Fornasiero, D., Ralston, J., Particle-bubble collision models - A review. Advances in Colloid and Interface Science, 2000, **85(2)**, 231-256.

Hinze, J.O., *Turbulence*. 1975, McGaw-Hill, New York.

Hu, C., Mei, R., 1997. Effect of inertia on the particle collision coefficient in Gaussian turbulence, In *The 7th International Symposium on Gas-Solid Flows, ASME Fluids Engineering Conference*, Vancouver, BC, Canada, pp. FEDSM97-3608.

Jameson, G.J., Nguyen, A.V., Ata, S., 2007. The flotation of fine and coarse particles, In *Froth Flotation: A Century of Innovation*, eds. Fuerstenau, M.C., Jameson, G.J., Yoon, R.-H. SME, Denver, CO, USA, pp. 329-351.

Kruis, F.E., Kusters, K.A., The collision rate of particles in turbulent flow. Chemical Engineering Communications, 1997, **158**, 201-230.

Lynch, A.J., Harbort, G.J., Nelson, M.G., *History of Flotation*. 2010, The Australasian Institute of Mining and Metallurgy, Burwood, Victoria, Australia.

Meyer, C.J., Deglon, D.A., Particle collision modelling – A review. Minerals Engineering, 2011, **24**, 719-730.

Napier-Munn, T.J., Wills, B.A., *Will's Mineral processing technology*. 2006, Butterworth Heinemann, Oxford.

Nguyen, A.V., An-Vo, D.-A., Tran-Cong, T., Evans, G.M., A review of stochastic description of the turbulence effect on bubble-particle interactions in flotation. International Journal of Mineral Processing, 2016, **156**, 75-86.

Nguyen, A.V., Schulze, H.J., *Colloidal Science of Flotation*. 2004, Marcel Dekker, New York.

Panchev, S., Haar, D.t., *Random Functions and Turbulence*. 1971, Pergamon Press, Oxford.

Pinsky, M.B., Khain, A.P., Grits, B., Shapiro, M., Collisions of small drops in a turbulent flow.

Part III: Relative droplets fluxes and swept volumes. Journal of the Atmospheric Sciences, 2006, **63(8)**, 2123-2139.

Pyke, B., Fornasiero, D., Ralston, J., Bubble particle heterocoagulation under turbulent conditions. J. Colloid Interface Sci., 2003, **265(1)**, 141-151.

Saffman, P.G., Turner, J.S., On the collision of drops in turbulent clouds. J. Fluid Mech, 1956, **1(1)**, 16-30.

Schubert, H., *Aufbereitung fester Stoffe, Band II, Sortierprozess*. 1996, Deutcher Verlag für Grundstoffindustrie, Stuttgart.

Schubert, H., On the turbulence-controlled microprocesses in flotation machines. Int. J. Miner. Process., 1999, **56(1-4)**, 257-276.

Schubert, H., Bischofberger, C., On the hydrodynamics of flotation machines. Int. J. Miner. Process., 1978, **5(2)**, 131-142.

Schubert, H., Bischofberger, C., On the microprocesses air dispersion and particle-bubble attachment in flotation machines as well as consequences for the scale-up of macroprocesses. Int. J. Miner. Process., 1998, **52(4)**, 245-259.

Taylor, G.I., Statistical theory of turbulence. Proceddings of the Royal Society A, 1935, **151**, 421-444.

Wang, L.P., Wexler, A.S., Zhou, Y., Statistical mechanical descriptions of turbulent coagulation. Physics of Fluids, 1998, **10(10)**, 2647-2651.

William, J.J.E., Crane, R.I., Particle collision rate in turbulent flow. International Journal of Multiphase Flow, 1983, **9(4)**, 421-435.

Yoon, R.-H., The role of hydrodynamic and surface forces in bubble-particle interaction. Int. J. Miner. Process., 2000, **58(1-4)**, 129-143.

Yuu, S., Collision rate of small particles in a homogeneous and isotropic turbulence. AIChE Journal, 1984, **30(5)**, 802-807.